Chromosome Res (2010) 18:851–872
DOI 10.1007/s10577-010-9170-7

Subnuclear targeting of the RNA-binding motif protein RBM6 to splicing speckles and nascent transcripts

Emma Heath · Fred Sablitzky · Garry T. Morgan

Received: 6 October 2010 / Revised: 1 November 2010 / Accepted: 2 November 2010 / Published online: 18 November 2010

Abstract RNA-binding motif (RBM) proteins comprise a large family of RNA-binding proteins whose functions are poorly understood. Since some RBM proteins are candidate alternative splicing factors we examined whether one such member of the family, RBM6, exhibited a pattern of nuclear distribution and targeting consistent with this role. Using antibodies raised against mouse RBM6 to immmunostain mammalian cell lines we found that the endogenous protein was both distributed diffusely in the nucleus and concentrated in a small number of nuclear foci that corresponded to splicing speckles/interchromatin granule clusters (IGCs). Tagged RBM6 was also targeted to IGCs, although it accumulated in large bodies confined to the IGC periphery. The basis of this distribution pattern was suggested by the targeting of tagged RBM6 in the giant nuclei (or germinal vesicles (GVs)) of *Xenopus* oocytes. In spread preparations of GV contents RBM6 was localized both to lampbrush chromosomes and to the surface of many oocyte IGCs, where it was confined to up to 50 discrete patches. Each patch of RBM6 labelling corresponded to a bead-like structure of 0.5–1 μm diameter that assembled de novo on the IGC surface. Assembly of these novel structures depended on the repetitive N-terminal region of RBM6, which acts as a multimerization domain. Without this domain, RBM6 was no longer excluded from the IGC interior but accumulated homogeneously within it. Assembly of IGC-surface structures in mammalian cell lines also depended on the oligomerization domain of RBM6. Oligomerization of RBM6 also had morphological effects on its other major target in GVs, namely the arrays of nascent transcripts visible in lampbrush chromosome transcription units. The presence of oligomerized RBM6 on many lampbrush loops caused them to appear as dense structures with a spiral morphology that appeared quite unlike normal, extended loops. This distribution pattern suggests a new role for RBM6 in the co-transcriptional packaging or processing of most nascent transcripts.

Keywords Lampbrush chromosome · nuclear body · interchromatin granule cluster · germinal vesicle · splicing factor

Abbreviations
CB Cajal body
CELF1 CUG-BP1 and ETR-3 Like Factor 1

Responsible Editor: Herbert Macgregor.

E. Heath · F. Sablitzky · G. T. Morgan (✉)
Centre for Genetics and Genomics, School of Biology,
University of Nottingham,
Queen's Medical Centre,
Nottingham NG7 2UH, UK
e-mail: garry.morgan@nottingham.ac.uk

Present Address:
E. Heath
Wellcome Trust Centre for Stem Cell Research,
University of Cambridge,
Tennis Court Road,
Cambridge CB2 1QN, UK

DRB	5,6-dichloro-1-β-D-ribofuranosylbenzimidazole
GV	Germinal vesicle
IGC	Interchromatin granule cluster
LBC	Lampbrush chromosome
pol II	RNA polymerase II
RBM6	RNA-binding motif protein 6

Introduction

Two important principles governing the mechanics and regulation of nuclear function have emerged recently. One concerns the structural organization of the nucleus into sub-compartments, many of which appear morphologically as diverse nuclear bodies. These compartments are sites that may coordinate and increase the efficiency of various nuclear processes such as gene expression and DNA repair and/or the biogenesis of the molecular machines that carry out these processes (reviewed by Misteli 2007; Matera et al. 2009). The second principle is the pronounced coupling of sequential stages of nuclear gene expression in which events such as RNA synthesis and the processing and export of transcripts appear to be integrated, primarily by co-transcriptional events that occur on nascent transcripts. Co-transcriptional coupling is also thought to allow the fates of transcripts in the cytoplasm to be pre-programmed in the nucleus (reviewed by Pawlicki and Steitz 2010). Evidence for the operation of both principles is provided by two types of nuclear compartment, namely nucleoli and the foci of RNA polymerase II (pol II) transcription also known as transcription factories (Cook 1999; Sutherland and Bickmore 2009). Both types of structure appear unusual among nuclear compartments in having an obligate association with specific DNA loci, namely pre-ribosomal RNA genes and protein coding genes, respectively, and they contain RNA-interacting factors involved in their cognate post-transcriptional processes. Other types of classic nuclear bodies can also be associated with genes, albeit transiently. Cajal bodies (CBs) are prominent in the nuclei of many, though not all, cell types, and are often associated with genes encoding small nuclear RNAs and histone mRNAs. The presence in CBs of splicing snRNPs and factors involved in the processing of various small RNAs suggests that one of the functions of CBs is in the assembly and maturation of the splicing machinery (reviewed by Gall 2003; Matera and Shpargel 2006). Another type of nuclear body, the splicing speckles or interchromatin granule clusters (IGCs) are also enriched in snRNP and non-snRNP splicing factors. IGCs appear to associate with highly active genes and although their function is debated, IGCs may be sites of spliceosome recycling (Hall et al. 2006).

Much of the evidence for the distribution of spliceosome components among multiple nuclear compartments has been obtained from mammalian cell lines. However the most direct demonstrations of their co-transcriptional interaction with active genes have come from investigations of polytene and lampbrush chromosomes (LBCs). Unlike the transcriptional foci of mammalian cell lines, in these giant chromosomes transcribed regions and, in the case of LBCs, even arrays of nascent transcripts can be resolved by light microscopy (reviewed by Daneholt 2001; Morgan 2002). Moreover, the high levels of morphological detail available in giant chromosomes has allowed the characterization of splicing factors that specifically associate in vivo with the transcripts of particular genes, such as the SR protein hrp45 in the polytene chromosomes of *Chironomus tentans* (Singh et al. 2006). Similarly, the RNA-binding protein CELF1 has been shown to exhibit a limited distribution among and even within the transcription units of lampbrush chromosome loops, which is consistent with its established role in regulating alternative splicing pathways (Morgan 2007). Such distributions support one proposed mechanism for regulated alternative splicing, namely one dependent on the cell type-specific expression of splicing activators that affect splicing of only a restricted number of genes (Black 2003). However, a second possible mechanism involves ubiquitously expressed splicing factors that normally repress alternative splicing but which are subject to gene-specific antagonism that gives rise to an up-regulated alternative splicing pattern (Lin and Tarn 2005). One straightforward means of distinguishing whether a putative splicing regulator functions as a gene-specific activator or as a general repressor is provided simply by assessing whether it is widely or narrowly distributed among the nascent transcripts of active transcription units.

Here we have used cell biological approaches to address in detail the nuclear distribution and hence the potential functional roles of one member of a novel class of RNA-binding proteins, the RBM (RNA-binding motif) family. Several of these proteins are thought to be splicing factors (reviewed by Sutherland et al. 2005). RBM proteins are evolutionarily conserved and contain one or more RNA-binding domains of the type designated RRM (RNA-recognition motif). The best characterised is RBM5, which was originally identified as a candidate tumour suppressor and has recently been shown to control alternative splicing pathways of apoptosis-related genes (Bonnal et al. 2008; Fushimi et al. 2008). Another family member, RBM4, is a multifunctional protein with co-transcriptional roles in both the regulation of splicing via antagonism of other splicing factors (Lai et al. 2003; Lin and Tarn 2005), and in the micro-RNA-mediated repression of translation (Hock et al. 2007; Lin and Tarn 2009). A less well-understood protein, RBM6 (also known as def-3; Drabkin et al. 1999; Hotfilder et al. 1999) has high sequence similarity with RBM5 and may also be a splicing factor involved in regulating apoptosis (Bonnal et al. 2008).

We have investigated the nuclear localization and targeting of RBM6 in order to assess its putative role in splicing in vivo. We found that in mammalian cultured cell lines endogenous and exogenous RBM6 was associated with IGCs, consistent with a role as splicing factor. Unexpectedly exogenous RBM6 accumulated at the periphery of the IGCs and a similar behaviour was found when the fate of RBM6 in *Xenopus* oocyte nuclei was examined. Here though it was clear that the peripheral localization was due to de novo formation of self-organizing nuclear structures on the IGC surface. The formation of these structures depended on the distinctive N-terminal domain of RBM6, a domain that we also show brings about multimerization/self-association of the protein. This property is shared with marker proteins associated with known nuclear bodies and may suggest common principles for the biogenesis of the novel RBM6-containing structures and nuclear bodies in general. The role of RBM6 as a general splicing factor was also suggested by its second site of accumulation in oocyte nuclei, namely on the nascent transcripts of LBC transcription units. RBM6 was distributed among the nascent transcripts of most loops, implying a role as a general factor, and it also brought about a unique alteration in the morphology of LBC loops.

Materials and methods

Constructs

Full-length mouse RBM6 cDNA was constructed from six partial cDNAs and was verified by sequencing. Expression clones were constructed in the following vectors: pRSET T7 (Invitrogen) for His-tagged RBM6, pcDNA3/MT (Smith et al. 2003) for *myc*-tagged proteins, the pEGFP-C series (Clontech) and pDsRed1-C1 (Clontech).

Tissue culture and transfection

HeLa, COS-7, and NIH 3T3 cell lines were grown in complete media and transiently transfected using the non-liposomal lipid transfection reagent Effectene (Qiagen) according to the manufacturer's recommendations. Cells were incubated for between 12–48 h to allow expression of the fusion protein. For treatment with inhibitors cells growing on coverslips were placed in complete medium containing 5 μg/ml actinomycin D (Sigma) or 100 μM 5,6-dichlorobenzimidazole riboside (DRB; Sigma) or 20 μg/ml cycloheximide (Sigma) and incubated for 3 h.

Immunoblotting

Whole cell lysates were prepared from both untransfected cells and from transfected COS-7 cells 48 h post-transfection. Cells were washed with 1× phosphate buffered saline (PBS), trypsinized and pelleted by centrifugation at 3,000×*g* for 3 min. The cell pellet was then resuspended in 50–200 μl of protein lysis buffer (50 mM Tris (pH 7.4), 150 mM NaCl, 2 mM EDTA (pH 8.0), 10% Triton-X-100, 1× complex proteinase inhibitors (Roche)), incubated for 10 min on ice and centrifuged at 4°C for 1 min at 12,000 rpm in a microcentrifuge. After addition of an equal volume of 2× Laemmli buffer (100 mM Tris (pH 6.8), 20% glycerol, 4% sodium dodecyl sulfate (SDS), bromophenol blue, 10% β-mercaptoethanol) to the supernatant, samples were denatured by heating at 90°C for 3 min, quick chilled on ice and then stored

at −20°C until required. Samples were subjected to SDS-polyacrylamide gel electrophoresis (SDS-PAGE) essentially as described (Laemmli 1970), after which proteins were electroblotted onto ECL-nitrocellulose membrane (Hybond). Blots were stained with Ponceau-S (Sigma) and then blocked with 5% milk powder in 1× PBS plus 0.05% Tween-20 for 1 h. Membranes were incubated in the appropriate primary antibody diluted in 5% milk/1× PBS/T for 1 h, rinsed in 1× PBS/T and then incubated for a further 1 h with anti-rabbit horseradish peroxidase (HRP) conjugate or anti-mouse HRP conjugate diluted in 5% milk/1× PBS/T. After washing signals were detected using the ECL detection system (Amersham), according to the manufacturer's instructions.

Cytological preparation and analysis of cultured cell lines

Immunofluorescence staining was carried out on cultured cells grown on coverslips and fixed in 4% (*w*/*v*) paraformaldehyde for 10 min. Following fixation, cells were permeabilized with 0.5% Triton-X-100 (BDH) in 1× PBS for 2 min on ice. Coverslips were then rinsed with 1× PBS for 5 min and incubated in 10% fetal calf serum (FCS) in 1× PBS for 30 min. Cells were incubated with the appropriate primary antibody (diluted in 10% FCS in 1x PBS, see below), washed with 10% FCS in 1× PBS and incubated with the secondary antibody for 1 h prior to washing and incubation in 2 mg/ml DAPI. For antibody α−PSP-1 permeabilization was increased to 15 min on ice with 1% Triton-X-100, and 0.05% Tween-20 (Sigma) in 1× PBS was used in the blocking and incubation steps. Primary antibodies were diluted as follows: anti-RBM6 rabbit polyclonal antisera α83 and α84 (from R. Dikstein), 1:50 to 1:1,000; mAb SC35 (Sigma) 1:2,000; α*myc* mAb 9B11 (Cell Signalling Technologies) 1:400; antiserum R508 (Chan et al. 1994) 1:200; α−PSP-1 (from A. Lamond) 1:50. Alexa 488- and 546-labelled secondary antibodies (Molecular Probes) were used at 2 μg/ml. Cells expressing fluorescent proteins were fixed with paraformaldehyde and permeabilized with Triton-X-100 as above.

Wide-field fluorescence microscopy of fixed cells was performed using an Axioskop 2 MOT microscope (Carl Zeiss) and images captured with an Axiocam CCD camera and supporting Axiovision 2.05 software (Carl Zeiss). For confocal microscopy an LSM510uv Kombi confocal on an Axiovert 100 inverted microscope (Carl Zeiss) was used. For each nucleus, typically 15–20 optical sections were recorded and images presented are selected optical sections from the Z-stack. All image data were processed using the LSM510 software (Carl Zeiss).

Expression of RBM6 in *Xenopus* oocytes

His-tagged RBM6 constructs were made in pRSET vectors and then verified for their ability to encode intact polypeptides of the predicted size by using them to produce ^{35}S-labelled proteins in a coupled transcription/translation system followed by SDS-PAGE and fluorography (as described in detail in the final section below). Capped sense-strand transcripts were prepared by using a mMessage mMachine kit (Ambion Inc.) to transcribe linearized plasmid DNAs with T7 RNA polymerase according to the manufacturer's instructions. The RNA was resuspended in RNase-free H_2O and concentration and sizes estimated by agarose gel electrophoresis. Separated stage IV or V oocytes for injection were prepared from small ovary fragments by treatment with 1 mg/ml collagenase (Type II; Sigma) in calcium-free OR2 saline (82.5 mM NaCl, 2.5 mM KCl, 1 mM $MgCl_2$, 1 mM Na_2HPO_4, and 5 mM HEPES; pH 7.4)) for about an hour, followed by rinsing in OR2 (including 1 mM $CaCl_2$). Oocytes were injected with 20 ng of RNA (1 μg/μl) into the cytoplasm and incubation at 19°C continued for the periods stated below.

Preparation and immunostaining of oocyte nuclear spreads

Nuclei (germinal vesicles (GVs)) of injected and uninjected control oocytes were manually dissected in GV isolation medium (83 mM KCl, 17 mM NaCl, 6.5 mM Na_2HPO_4, 3.5 mM KH_2PO_4, 1 mM $MgCl_2$, and 1 mM DTT; pH 7.0–7.2). Spread preparations of GV contents were made using the procedure developed by Gall (Gall 1998). After centrifugation to attach the GV contents to a microscope slide, preparations were fixed for a minimum of 1 h and a maximum of 16 h in 2% paraformaldehyde made up in PBS (137 mM NaCl, 2.7 mM KCl, 10.2 mM Na_2HPO_4, and 1.8 mM KH_2PO_4; pH 7.4) containing 1 mM $MgCl_2$.

Fixed preparations were rinsed in PBS and blocked by incubation in 5% normal goat serum (NGS; Jackson Immunoresearch Laboratories) in PBS for 15 min. The spreads were then incubated for 1 h at room temperature with primary antibodies, rinsed briefly with 5% NGS and then incubated for 1 h with secondary antibodies diluted in PBS. Finally, preparations were mounted in 50% glycerol/PBS. Primary antibodies were diluted in 5% NGS as follows: αHis6 mAb (Clontech), 5 μg/ml; mAb H5 (Warren et al. 1992) culture supernatant 1:50 dilution. Secondary antibodies, used at dilutions of 1–5 μg/ml, were Alexa 488-conjugated goat anti-mouse IgG, Cy3-conjugated goat anti-mouse IgM (Chemicon International), and Cy2-conjugated goat anti-mouse Fc (gamma) fragment (Jackson Immunoresearch Laboratories). Phase contrast and fluorescence observations were made with an Olympus BX-60 microscope as described previously (Smith et al. 2003). Images were captured with a Princeton Instruments digital CCD camera (Roper Scientific) using IPLab imaging software (Scanalytics Inc) and processed with iVision-Mac (BioVision Technologies) and Adobe Photoshop and Illustrator (Adobe Systems Inc).

In vitro pull-down assay

Method adapted from (Pellizzoni et al. 2002). Five micrograms of purified His-tagged fusion protein coupled to agarose was washed two times with 500 μl of pull-down buffer (PBB; 20 mM Tris (pH 7.5), 150 mM NaCl, 0.2% Triton-X-100). In parallel, ^{35}S-labelled proteins were produced from constructs that contained the T7 promoter using the TnT T7 Quick coupled transcription/translation system (Promega) according to the manufacturer's instructions. For the pull-down assay 10 μl of an in vitro transcription/translation reaction was added to 190 μl of PBB. The equilibrated ^{35}S-labelled protein was then added to the pre-washed His-tagged protein and incubated for 1 h at 4°C with rotation. The agarose-protein complexes were pelleted by centrifugation at 1,000 rpm for 10 s and washed four times with 500 μl of PBB. Bound proteins were eluted from the resin by addition of 10 μl of 4× Protein loading dye (Ambion). Samples were then boiled at 90°C for 3 min and analysed by SDS-PAGE followed by fluorography as follows. After treatment with Amplify fluorographic reagent (Amersham) for 30 min, gels were washed in destaining solution (7% methanol, 7% acetic acid, and 1% glycerol) before exposure for 5 h to Super RX film (Fuji) at −80°C.

Results

Localization and targeting of RBM6 in mammalian cell lines

The domain organization of mouse RBM6 is represented in Fig. 1. Rabbit polyclonal antisera were raised against a His-tagged truncated mouse RBM6 that contained both RRM domains and the intervening C4Zn-finger domain. Two polyclonal antisera, α83 and α84 were produced by Dr. R. Dikstein (University of Israel) and both used to detect proteins in whole cell protein extracts from HeLa, COS-7, and NIH3T3 cell lines by immunoblotting (Fig. 2a). Both antisera detected a major band of ~150 kDa in all three cell lines suggesting they recognize a protein corresponding to the full-length RBM6 (1,117 aa, MWt approximately 128 kDa). Antiserum α84 also detected an additional band of ~130 kDa in HeLa and COS-7 cell extracts. Both antisera α83 and α84 were used to immunostain mammalian cell lines (Fig. 2b, c) and showed that endogenous RBM6 was predominantly localized to the nucleus but with no apparent staining of nucleoli. Some differences in the pattern of intranuclear staining were observed between the two antisera. Antiserum α84 produced a number of discrete foci of staining throughout the interchromatin space, along with some diffuse staining of the nucleoplasm in HeLa cells and COS-7 cells. In contrast, antiserum 83 produced more diffuse RBM6 nucleoplasmic staining in these cell lines **(**Fig. 2b**)**. The different immunostaining patterns obtained suggest that different populations of endogenous RBM6 exist in vivo with each exhibiting different subnuclear localizations.

The nuclear foci of immunostaining of endogenous RBM6 produced by antiserum α84 resembled the 'splicing speckles' or IGCs found when cells are stained with antibodies against components of the splicing machinery (Spector 1993). We carried out co-immunostaining experiments using α84 together with antibodies specific for three different IGC components, namely an anti-Sm antibody (Y12; Lerner et al. 1981), the phosphorylated form of the non-snRNP splicing factor SC35 (Fu and Maniatis

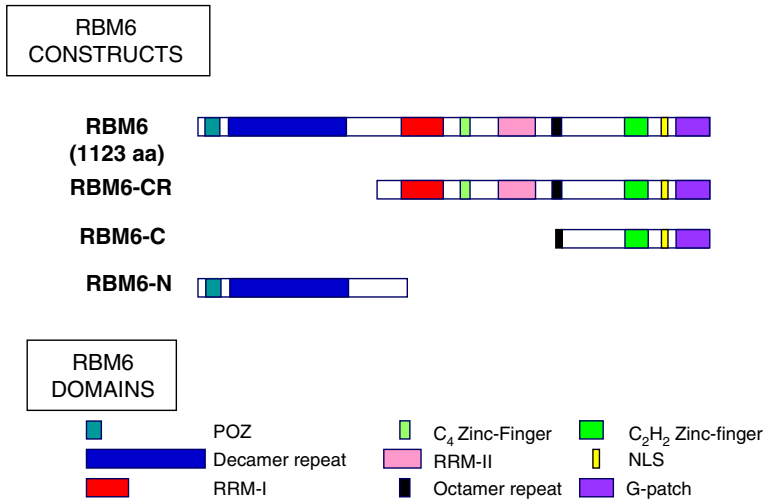

Fig. 1 Protein domain organization of RBM6 and recombinant constructs. *Top line* is a schematic representation of full-length RBM6, showing the conserved domain structure. Below are schematic diagrams of mouse RBM6 deletion constructs use to produce tagged RBM6 mutant proteins. At the bottom is a key to protein domains conserved across distinct RBM family members and species identified using the SMART and CDART search tools (Schultz et al. 1998)

1992; Fu et al. 1992), and the SR protein SF2/ASF (antibody AK103; Caceres et al. 1997). Clear overlap of the RBM6 foci and splicing speckles was apparent by confocal microscopy of the immunostaining obtained with SC35 (Fig. 2c) and the other antibodies. Co-localization of RBM6 and SC35 was also observed in COS-7 cells (data not shown). The presence of a subpopulation of endogenous RBM6 recognized by antiserum α84 in splicing factor speckles supports the suggestion that RBM6 functions in splicing or a related process. The significance of the more diffusely localized RBM6 fraction is considered below.

To examine the targeting behaviour of exogenous RBM6 we fused green fluorescent protein (GFP; Prasher et al. 1992) in-frame to the amino terminus of the full-length coding region of RBM6. In Western blots of whole cell extracts from transfected COS-7 cells a single protein band corresponding to the full-length fusion protein, was detected with both RBM6 antiserum α84 (Fig. 3a) and anti-GFP antibody (data not shown). To localize the RBM6/GFP fusion protein cell lines were transiently transfected with RBM6-GFP or a control GFP construct and 24 h later the cells were fixed and the subcellular distribution of GFP determined by fluorescence microscopy. In HeLa, COS-7, and NIH3T3 cells, RBM6-GFP localized to the nucleus and accumulated in a number of rather globular foci that were about 0.5 μm in diameter but varied in exact size and number in a given cell-population (Fig. 3b). Some diffuse fluorescence of the nucleoplasm but not the nucleolus was also detectable. The fluorescent foci were restricted to the interchromatin space found between areas of densely packed heterochromatin indicated by intense DAPI staining. The majority of cells transfected with the RBM6-GFP construct exhibited this distribution pattern and even cells with a relatively low level of RBM6-GFP expression displayed nuclear foci. Control GFP transfection showed that the unfused GFP tag was uniformly distributed throughout the nucleus with no preferential targeting to a particular cellular compartment (Fig. 3b).

RBM6 was also fused to the myc peptide tag and co-expressed in HeLa cells with GFP-RBM6. Both tagged forms of the protein showed an identical distribution in the nucleus (Fig. 3c) with a fraction being localized to numerous foci distributed throughout the nucleus, and another fraction diffusely distributed in the nucleoplasm but undetectable in nucleoli. Western analysis of whole cell extracts from COS-7 cells expressing the RBM6-myc fusion protein verified that the full-length protein was produced (Fig. 3a). A fusion of RBM6 with the red fluorescent protein DsRed also produced a similar distribution pattern to that seen with RBM6-GFP (not shown). Overall, all three constructs show that exogenous RBM6 forms nuclear foci in mammalian cultured cells and these foci will be referred to as RBM6 bodies. The distribution of exogenous RBM6 initially appeared to resemble closely that of the endogenous RBM6 recognized by antiserum α84 and since the latter localizes to IGCs splicing, we asked whether RBM6-GFP was similarly targeted. We immunostained HeLa cells that were transiently expressing

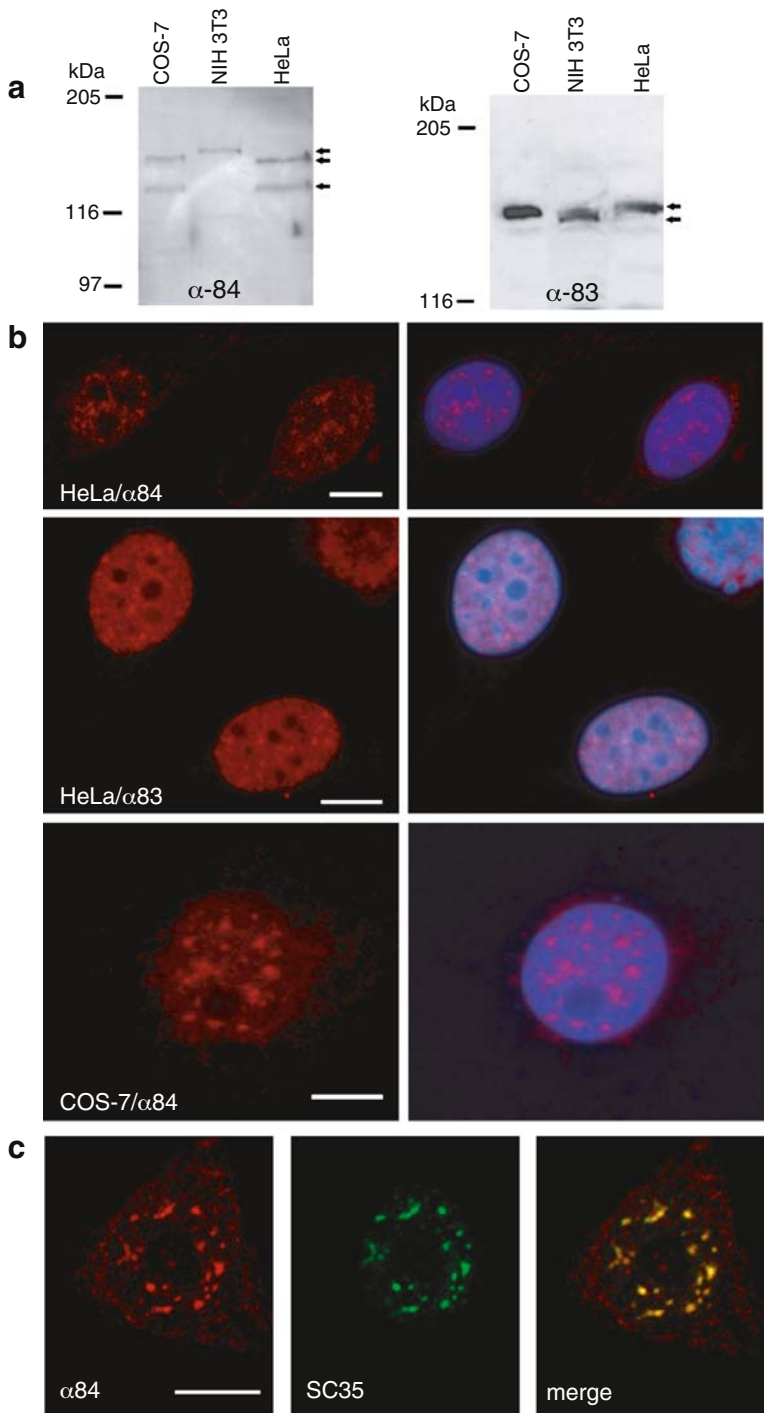

Fig. 2 Localization of endogenous RBM6 in mammalian cell lines. **a** Whole cell extracts from HeLa, NIH 3 T3 and COS-7 cells were subjected to SDS-PAGE and transferred to nitrocellulose. Immunoblots were probed with RBM6 antisera α83 or α84. *Arrows* indicate the different RBM6 protein isoforms. **b** *Left-hand panels* show localization of endogenous RBM6 in HeLa and COS-7 cells by indirect immunofluorescence with antisera α83 or α84 (*red*). *Right-hand panels* show overlay of DAPI stain and RBM6 immunostain. α84 images are 1.14 μm confocal slices, α83 image by wide-field microscopy. **c** HeLa cell co-immunostained with antiserum α84 for RBM6 (*red*) and mAb SC35 for IGCs (*green*). Co-localized RBM6 and SC35 immunostaining indicated as *yellow* in merged image. Images are 0.41 μm confocal sections. Scale bars, 10 μm

RBM6-GFP with anti-SC35 antibody to detect IGCs (Fig. 4a) but surprisingly, no overlap of RBM6 with the SC35 domains was detected. However, closer inspection of optical *z* sections of the double-labelled nuclei showed that the RBM6-GFP bodies were frequently adjacent to IGCs with typically a pair of RBM6 bodies associated with a single IGC (Fig. 4a, enlargement). Hence the overexpressed RBM6 present in RBM6 bodies appears to be excluded from, but often localized adjacent to, splicing speckles. Interestingly,

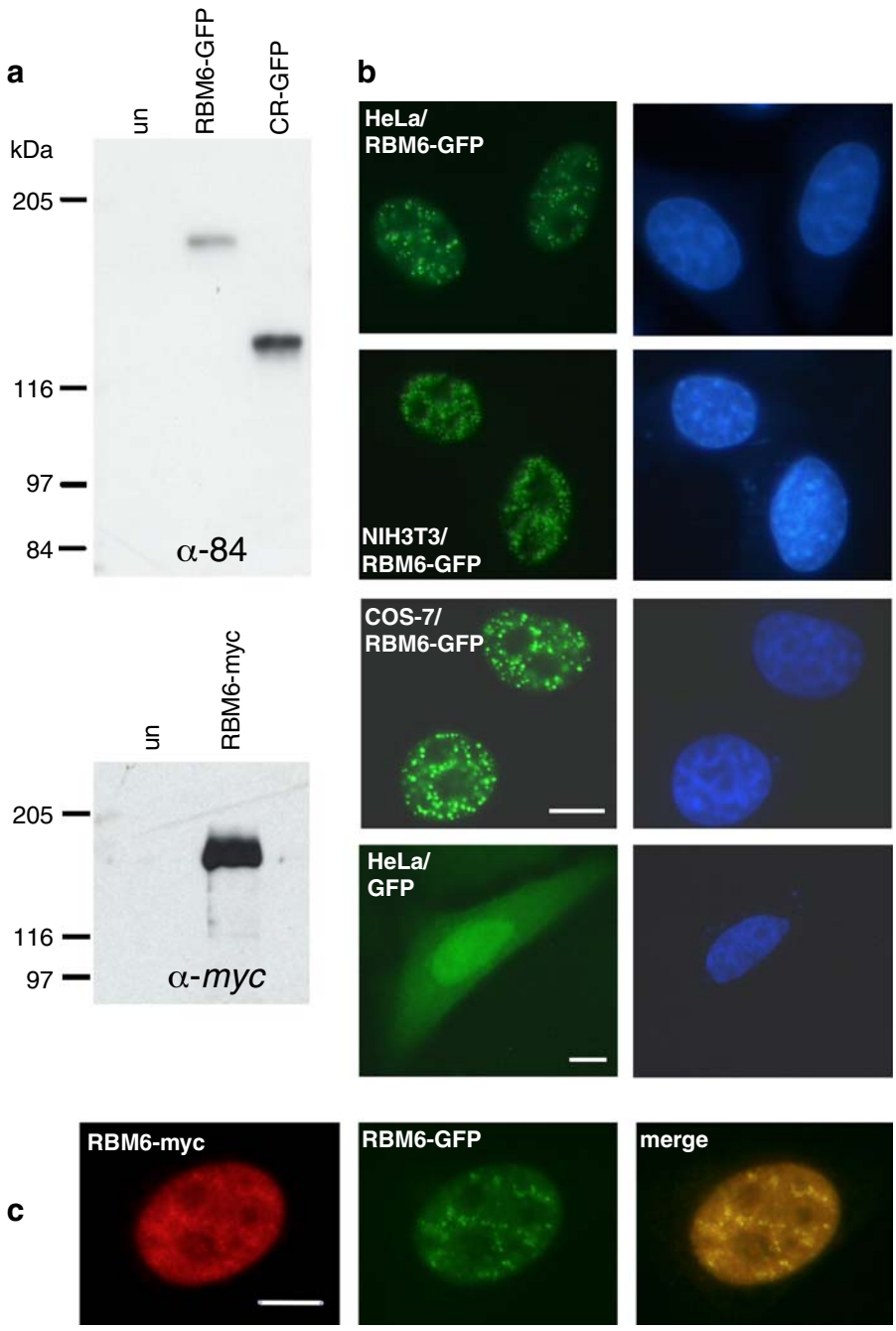

Fig. 3 Expression of recombinant RBM6 in cultured cell lines. **a** Immunoblots of whole cell extracts from COS-7 cells expressing fusions of RBM6 or its CR deletion with GFP or myc tags. *Control lanes* (*un*) contain extract from untransfected cells. Blots were probed with either the RBM6 antiserum α84 or an anti-myc antibody as indicated. Molecular weight markers are in kDa. **b** Mammalian cell lines as indicated were transiently transfected with either an RBM6-GFP fusion construct or GFP alone and the exogenous proteins localized by GFP fluorescence (*green*). The *right-hand panels* show DAPI staining (*blue*) of the corresponding cell nuclei. **c** A HeLa cell co-transfected with RBM6-myc and RBM6-GFP constructs and then imaged for immunofluorescence after staining with a myc-tag monoclonal antibody (*red*) and for GFP fluorescence (*green*). Co-localization of the fusion proteins indicated by yellow in the merged image. Scale bars, 10 μm

the closely related protein, RBM10 and its GFP-tagged derivative are also found in large nuclear bodies at the IGC periphery in a variety of mammalian cell types (Inoue et al. 2008)

The difference between the localization of endogenous RBM6 within speckles and that of the exogenous protein in RBM6 bodies might be due to the peripherally localized RBM6 bodies representing pre-existing speckle-associated structures that contained a fraction of endogenous RBM6 protein undetected by either of the polyclonal antisera. One well-documented example of a nuclear factor that localizes adjacent to IGCs is PSP1, which is the signature protein of a class of nuclear bodies found in

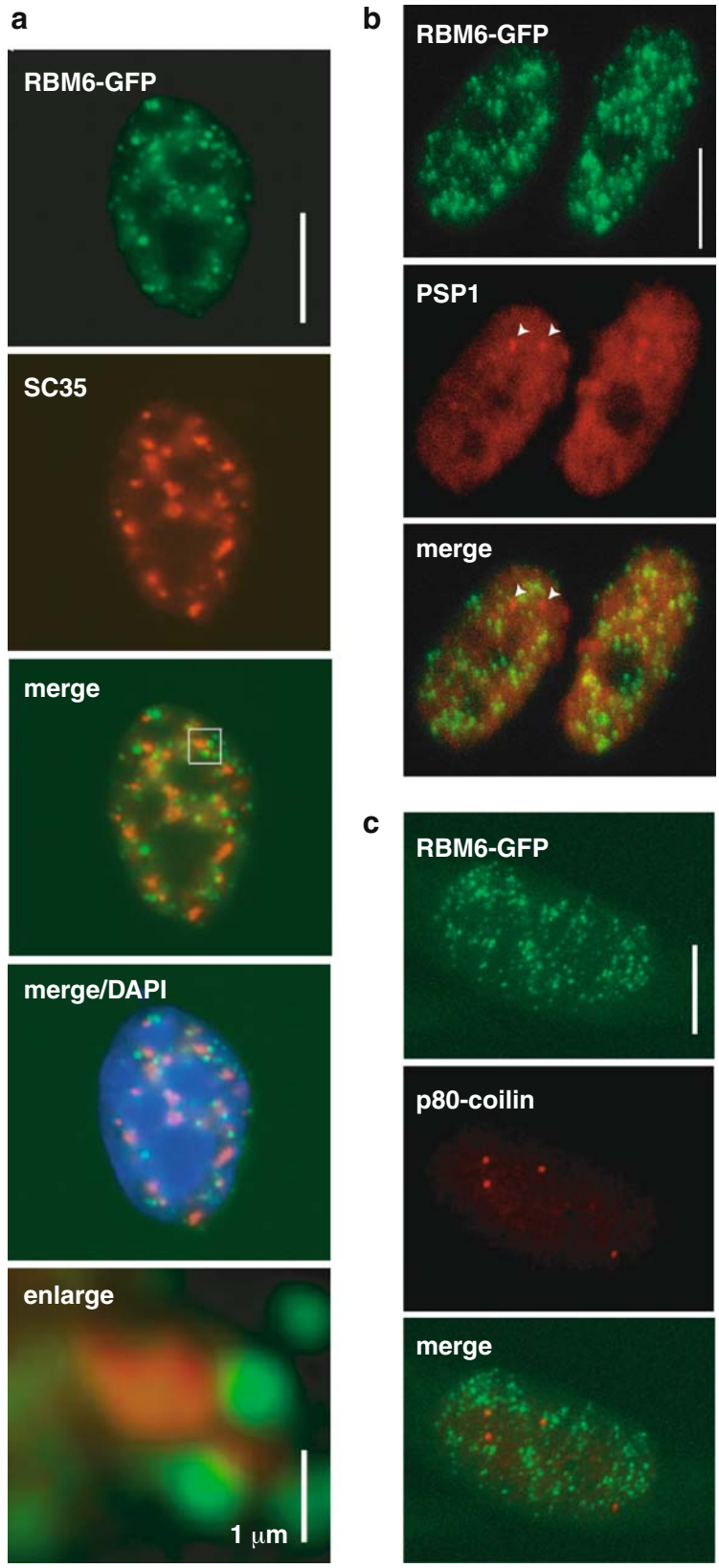

Fig. 4 Spatial relationship of RBM6 bodies and other mammalian nuclear bodies. **a** HeLa cells transiently transfected with RBM6-GFP to show RBM6 bodies (*green*) and immunostained with mAb SC35 to identify IGCs (*red*). In the merged images the two types of compartment appear adjacent but show little overlap (*yellow*). An enlargement of the *boxed area* indicated in the merged image shows two RBM6 bodies at the periphery of an IGC. **b** HeLa cells transiently expressing RBM6-GFP (*green*) were immunostained with PSP1 antiserum (*red*) to identify paraspeckles (examples indicated by *arrowheads*). The distinct localizations of the two types of body are indicated by the absence of *yellow* objects in the merged image. **c** HeLa cells transiently expressing RBM6-GFP (*green*) immmunostained for p80-coilin using antiserum R508 to identify Cajal bodies (*red*). Merged images (0.41 μm confocal sections) show a lack of co-localization (*yellow*) of the two types of body. Scale bars, 10 μm except where indicated

close proximity to IGCs termed paraspeckles (Fox et al. 2002). To test if RBM6 bodies represented paraspeckles, HeLa cells transiently expressing RBM6-GFP were immunostained with anti-PSP1 antiserum. In these nuclei, endogenous PSP1 was localized in punctate structures corresponding to paraspeckles that were distributed throughout the nucleoplasm (Fig. 4b). However from the merged image of PSP1 staining and RBM6-GFP fluorescence (Fig. 4b, merge), it appears that there is no overlap between RBM6 bodies and paraspeckles. We also examined whether some RBM6 bodies might represent the accumulation of exogenous RBM6 in two other well-characterised subnuclear compartments, CBs and PML bodies. The distribution of RBM6-GFP with respect to CBs was analysed using an antiserum against the marker protein p80 coilin (Andrade et al. 1991). This showed that the bright nuclear foci characteristic of CBs did not overlap or associate with RBM6 bodies (Fig. 4c). Similarly a lack of association was observed for RBM6 and PML bodies, which were identified using a PML-GFP fusion protein as a marker (not shown).

Although our search has not been exhaustive, the failure to identify the foci of exogenous RBM6 accumulation in known nuclear bodies could indicate that RBM6 bodies are in fact novel, self-organizing nuclear structures assembled de novo. To obtain further insight into the biogenesis of RBM6 bodies we next examined the targeting behaviour of mouse RBM6 in the distinctive type of nucleus found in oocytes of the frog, *Xenopus*.

Targeting of RBM6 in oocyte nuclei

The giant nucleus, or GV, of an amphibian oocyte has proved a valuable system for the study of nuclear structure and function (Gall et al. 2004), primarily because of the large size and consequent extraordinary levels of morphological detail exhibited by its nuclear structures. The latter include the highly extended and transcriptionally active LBCs, about a thousand extrachromosomal nucleoli and 50–100 huge CBs, which recent evidence suggests may actually represent a particular subtype of coilin-containing structure, namely the histone locus body (Liu et al. 2009). Moreover the most numerous organelles in the GV are thousands of smaller bodies that correspond to IGCs. Originally called B-snurposomes because of their enrichment for splicing snRNPS (Gall 1991), the IGCs of Xenopus GVs are spherical bodies of ~1–4 μm in diameter composed of dense particles that closely resemble the interchromatin granules found in the splicing speckles of somatic nuclei (Gall et al. 1999). Intriguingly, and for reasons that are not understood, oocyte IGCs are often intimately associated with CBs, occurring either inside or attached to the surface of the larger bodies.

To follow the targeting of mouse RBM6 in Xenopus oocytes we made a His-tagged, full-length RBM6 construct (RBM6-His) from which synthetic RNAs were transcribed in vitro and then microinjected into the oocyte cytoplasm. After incubation of injected oocytes for 24–48 h to allow for RBM6 expression we prepared cytological spreads of the contents of manually isolated GVs and processed them for immunostaining. Using an antibody against the His-tag, two types of structure exhibited intense and specific immunostaining for RBM6 (Fig. 5a); these were (1) the typical loops as well as giant marker loops of the LBCs (described in the final Section below) and (2) most of the IGCs. The immunostaining pattern of His-tagged RBM6 in IGCs appeared peripheral and distinctly punctate, being limited to discrete surface patches that varied in number from several to about 50 per IGC (Fig. 5a, c). A similar immunostaining pattern has been described for a variety of endogenous hnRNP proteins (Roth et al. 1990; Wu et al. 1991; Pyne et al. 1994). Both free IGCs and those on the surface of CBs exhibited peripherally distributed RBM6 beads although IGCs contained within CBs did not (Fig. 5c). Only rarely did CBs themselves or nucleoli exhibit any similar patches of immunostaining and we think these are due to non-specific sticking of nucleoplasmic RBM6 accumulations. Overall then, in amphibian oocytes exogenous mouse RBM6 was specifically targeted to the same location in the equivalent nuclear bodies as described above for mammalian cultured cells, namely the surface of IGCs.

The nature of RBM6 targeting became apparent when preparations were examined by differential interference contrast (DIC) microscopy. The His-tagged protein detected by immunostaining was confined to discrete, roughly spherical structures of ~0.5–1 μm diameter attached to the IGC surface (we will refer to these as RBM6 beads). Since such structures are not normally present on the surface of

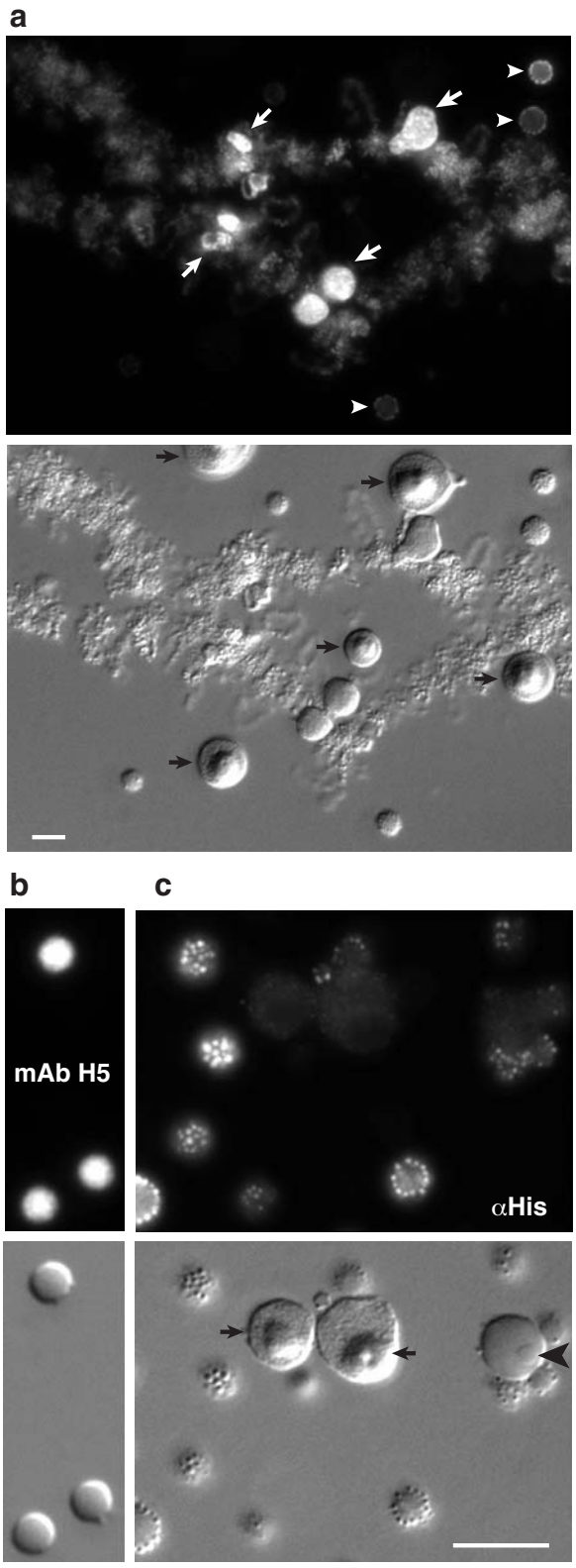

Fig. 5 Subnuclear targeting of RBM6 in *Xenopus* oocytes. **a** Distribution of His-tagged RBM6 among nuclear structures isolated from an oocyte injected 48 h previously with synthetic RNA encoding RBM6-His. *Upper image*, obtained by immunostaining with αHis mAb, shows a portion of a lampbrush bivalent with highly stained, giant loop-derived "marker" structures present on the two homolgoues at two separate loci (*arrows*) and general staining of extended and collapsed lateral loops along the length of the chromosome axes. Also exhibiting varying amounts of surface or peripheral staining for RBM6 are the oocyte equivalents of IGCs that exist free of the chromosomes (*arrowheads*). The lower differential interference contrast (DIC) image shows extrachromosomal nucleoli (*arrows*) that are unstained for RBM6 in the upper image. **b** IGCs isolated from an uninjected control oocyte. The *upper image* shows IGCs immunostained homogeneously with mAB H5, which in addition to pol II, recognizes a phosphorylated serine epitope in an unknown RNP (Doyle et al. 2002) and can be used to identify IGCs specifically among the various oocyte nuclear bodies. The lower, DIC image shows the normal smooth morphology of oocyte IGCs. **c** IGCs isolated from oocytes expressing RBM6-His. The upper fluorescence image shows the distribution of RBM6-His after immunostainng with αHis mAb and the lower is a DIC image of the same field. Multiple globular RBM6 beads attached to the surface of the IGCs are visible by DIC and correspond to the bright foci in the punctate IGC immunostaining pattern. Also present in the DIC image are nuclear bodies that are not immunostained for RBM6-His nor exhibit attached RBM6 beads; indicated are nucleoli (*small arrows*) and a Cajal body containing an internalised IGC (*arrowheads*). Note that three external IGCs associated with this CB do exhibit a variable number of stained RBM6 beads on their surface. Scale bars, 10 μm

oocyte IGCs (Fig. 5b), it seems that exogenous RBM6 assembles into these novel nuclear bodies de novo rather than being targeted to pre-existing large surface structures. Interestingly, sub-microscopic granular structures of around 100-nm diameter have been shown by electron microscopy normally to be attached to the surface of IGCs (Pyne et al. 1994) and conceivably these might form foci for the formation of RBM6 beads. Alternatively, the formation of RBM6 beads on oocyte IGCs (and perhaps also RBM6 bodies on somatic IGC surfaces) could be due simply to the spontaneous assembly of specifically targeted RBM6 into structures that are physically too large to penetrate the IGCs. This is notwithstanding that oocyte IGCs have been found by interferometry to be low-density structures and can be penetrated by molecules as large as 2,000 kDa dextran. (Handwerger et al. 2005). Similarly, the physical exclusion of RBM6 beads from Cajal bodies (which, like IGCs, are rather porous, sponge-like bodies; Handwerger et al. 2005) seems the most likely explanation for the absence of RBM6 from

the surfaces of those IGCs that occur as inclusions inside CBs.

To examine further the mechanisms of RBM6 targeting to the IGC surface and the factors governing the self-organization of RBM6 beads we next tried to identify which regions of the protein were involved. Two His-tagged RBM6 deletion constructs were made (Fig. 1): one, RBM6-CR-His, lacked just the N-terminal decamer repeat and POZ domains whereas the other, RBM6-C-His comprised a smaller C-terminal region consisting mainly of the C-terminal C_2H_2 zinc finger and G-patch domains. After injection of synthetic transcripts into the oocyte cytoplasm and incubation for 48 h, immunostaining with an anti-His-tag antibody revealed strong staining of IGCs (Fig. 6). However, unlike the situation with full-length RBM6, both deletion constructs were now targeted to the IGC interior and were fairly homogeneously distributed rather than exhibiting a patchy distribution on the surface. Moreover, these truncated forms of RBM6 also were able to accumulate within those IGCs present as inclusions in CBs (Fig. 6b). Hence it is striking that in amphibian oocytes these exogenous forms of RBM6 exhibit the same targeting pattern as endogenous RBM6 in mammalian cell lines, namely within IGCs. The crucial determinant of the altered targeting behaviour of the truncated versus full-length RBM6 is clear by DIC microscopy (Fig. 6). Neither of the RBM6 mutants formed the bead-like structures on the IGC surface that are seen with the full-length construct, and this we assume allows RBM6 molecules in smaller complexes, perhaps even as monomers, to penetrate IGCs and to distribute within them fairly homogeneously. Similarly, because it does not assemble into RBM6 beads, deleted RBM6 appears able to penetrate CBs and to target IGC inclusions within the CB. The ability of even the smallest deletion construct, RBM6-C-His, to still be targeted to IGCs suggests that the targeting specificity resides in the C-terminal domains of RBM6, presumably because this region is able to interact with an IGC component(s). Conversely, the formation of large, self-assembling particles on the IGC surface by full-length RBM6 requires its N-terminal region, suggesting that this region contains a domain with a multimerization function.

The RBM6 N-terminal region is a multimerization domain required for the formation of RBM6 bodies

To test whether multimerization of exogenous RBM6 could also explain the assembly of RBM6-bodies in cell lines, and in particular whether the N-terminal domain was required, RBM6 deletion constructs (Fig. 1) were cloned downstream of either the GFP or DsRed reporter gene. Constructs encoding either the full-length or mutant proteins were transiently expressed in HeLa cells and their subnuclear locali-

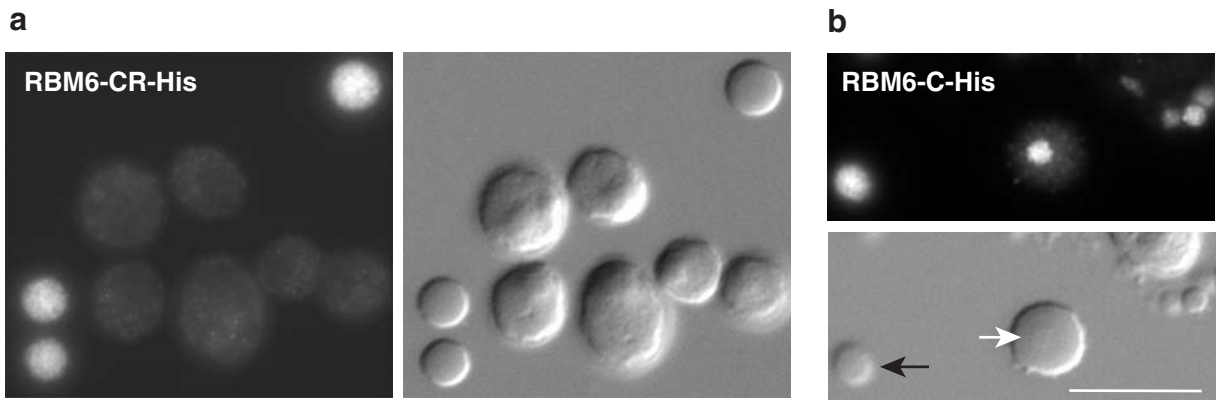

Fig. 6 Targeting of RBM6 deletion constructs to oocyte IGCs. **a** Nuclear structures isolated from an oocyte injected 48 h previously with synthetic RNA encoding the deletion mutant RBM6-CR-His. The fluorescent image, obtained by immunostaining with αHis mAb, shows RBM6-CR-His staining distributed throughout IGCs but absent from the cluster of six nucleoli visible in the corresponding DIC image. **b** Subnuclear distribution of RBM6 in an oocyte injected 48 h previously with synthetic RNA encoding the deletion mutant RBM6-C-His and immunostained with α-His mAb (*upper image*). In the DIC image below, a free IGC is indicated with a *black arrow* and an IGC contained within a CB with a *white arrow*. Scale bars, 10 μm

zation compared by direct fluorescence microscopy. Notably, a fusion protein lacking the N-terminal decamer repeat and POZ domains (RBM6-CR-GFP) localized to the nucleus but in a significantly more diffuse pattern than full-length RBM6-GFP (Fig. 7a). In approximately 50% of the cells analysed small

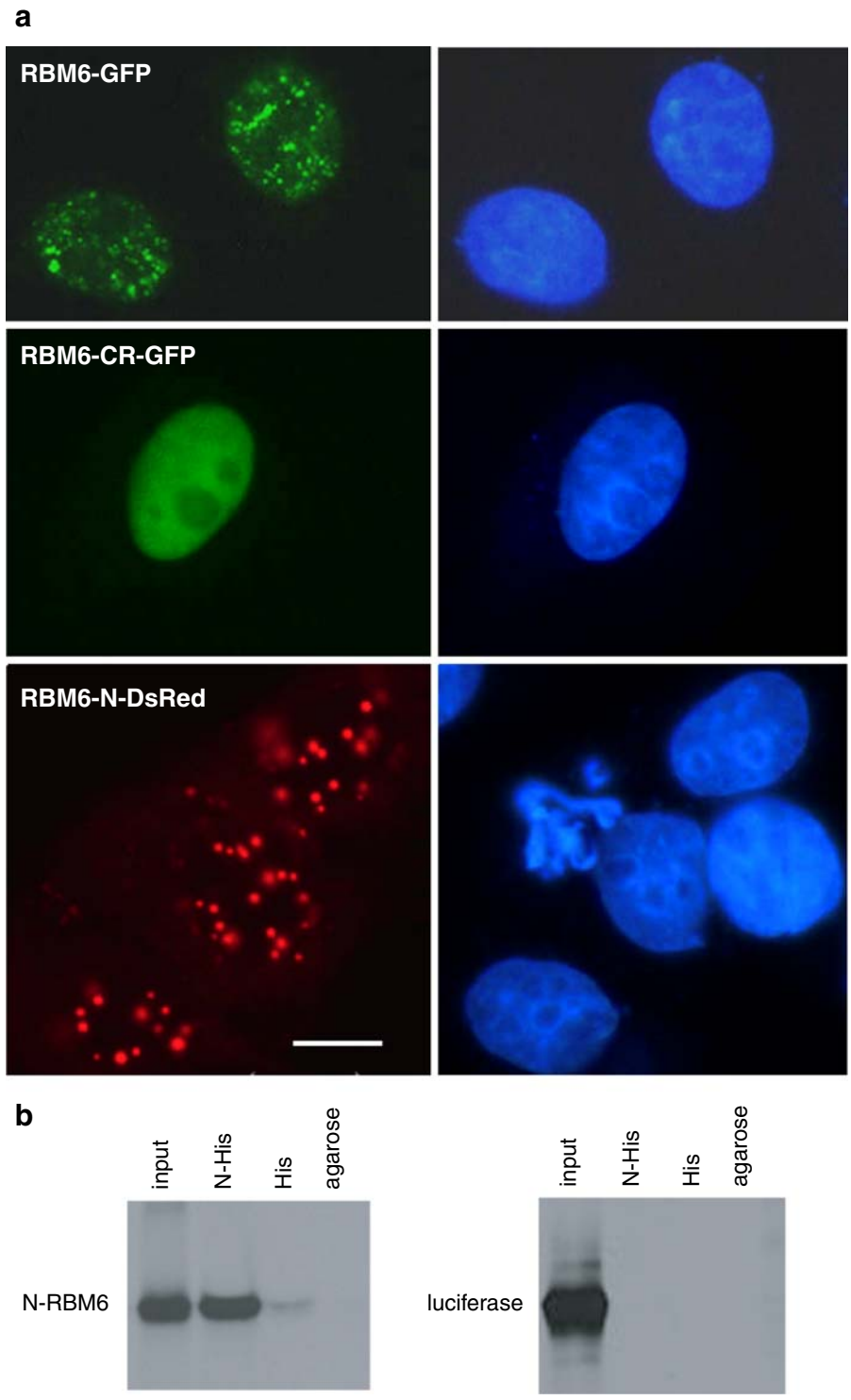

Fig. 7 Role of the RBM6 N-terminal domain in self-association. **a** HeLa cells transiently transfected with the indicated GFP- or DsRed-tagged RBM6 constructs (see Fig. 1 for detail). Self-association of each construct assayed by formation of multiple nuclear RBM6 bodies visualised by GFP (*green*) or DsRed (*red*) fluorescence. DAPI-staining channel shown in *right-hand panels*. Scale bar, 10 μm. **b** An in vitro protein pull-down assay using a truncated His-tagged RBM6 protein (*N-His*) comprising the N-terminal POZ and decamer repeat regions bound to agarose beads. Interaction of N-His with [^{35}S] methionine-labelled RBM6 N-terminal domain (*N-RBM6*) or control luciferase polypeptide assayed by SDS-PAGE and fluorography. Binding controls comprise the His-tag alone or agarose beads alone and the input lane represents 20% of the ^{35}S-labelled protein used in each pull-down assay

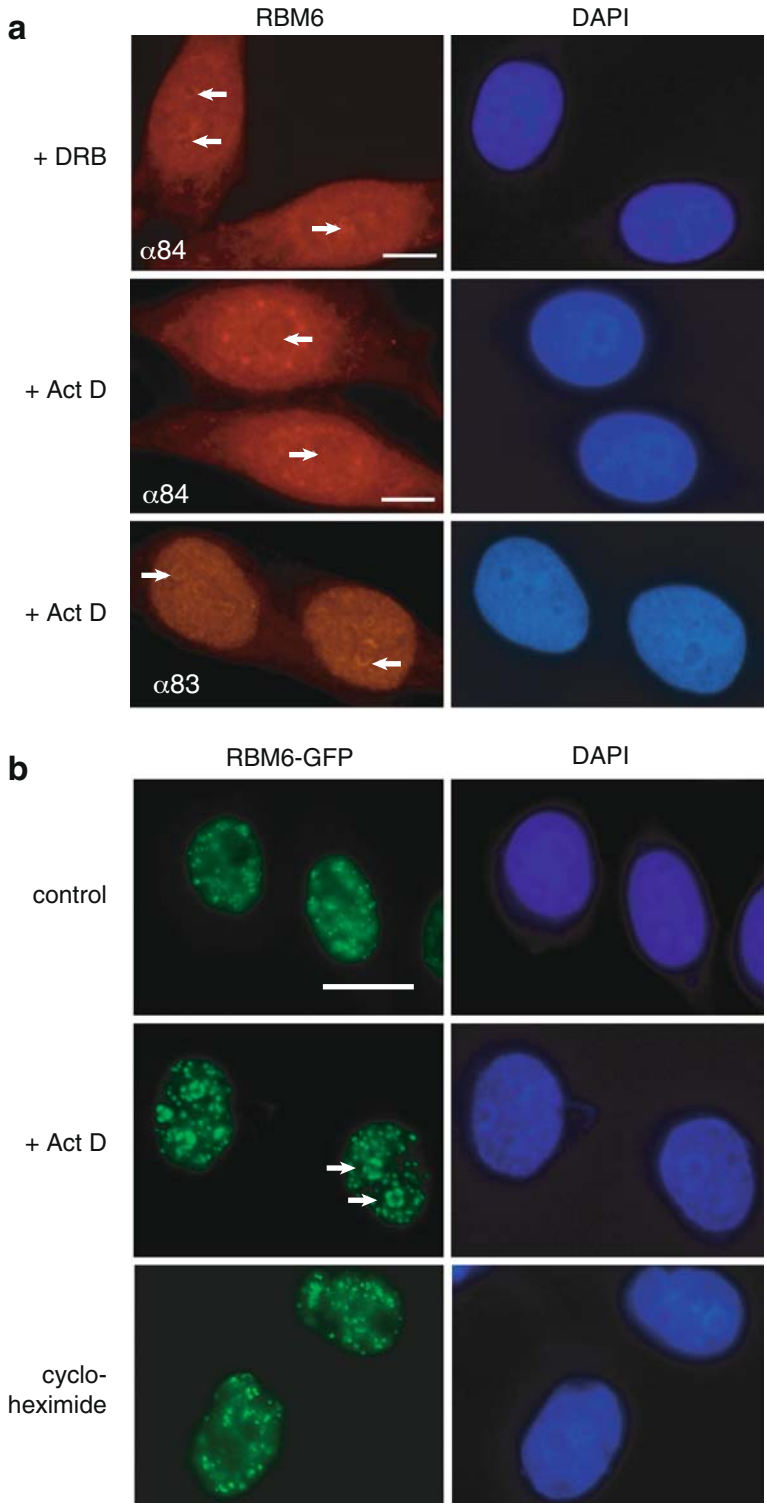

Fig. 8 Nucleolar relocalization of RBM6 during transcriptional inhibition. **a** HeLa cells were treated with 5 μg/ml Actinomycin D or 100 μM DRB for 3 h prior to fixation and the localization of endogenous RBM6 (*red*) determined by immunostaining with either antisera α83 or α84. *Arrows* indicate a sub-fraction of RBM6 that re-localized to the nucleolar periphery. DAPI staining (*blue*) is shown on the right. **b** HeLa cells transiently expressing RBM6-GFP (*green*) were incubated in media containing the transcriptional inhibitor, Actinomycin D (5 μg/ml) for 3 h or the protein synthesis inhibitor, Cycloheximide (20 μg/ml) for 3 h, prior to fixation. The distributions of the fusion proteins were determined by GFP fluorescence in both treated and untreated control cells (*green*). *Arrows* indicate a sub-fraction of RBM6-GFP that re-localized to the nucleolar periphery in actinomycin D-treated cells. DAPI staining (*blue*) shown in the *right-hand panels*. Scale bars, 10 μm

nuclear foci were visible, while in the remaining cells staining was diffusely nucleoplasmic with occasionally one or two large nuclear foci. A similar diffuse pattern was seen with the RBM6-C-GFP fusion protein, consisting of the C-terminal C_2H_2 and G-patch domains (not shown). On the contrary, construct N-DsRed comprising the N-terminal region of RBM6 but not the C-terminal region formed foci resembling RBM-6 bodies and did not exhibit a diffusely nucleoplasmic distribution (Fig. 7a). These results indicate that, as in oocyte nuclei, the N-terminal domain of RBM6 is required for the formation of subnuclear bodies in HeLa cells and implicate this region as being capable of bringing about multimerization of the exogenous protein. Indeed we think nuclear localization of the N-DsRed construct, which lacks the NLS sequence predicted for RBM6 (Fig. 1), may be explained by multimerization interactions between the N-terminal construct and the N-terminal domain of endogenous, full-length RBM6 proteins.

To show that the N-terminal domain of RBM6 can self-associate, an in vitro pull-down binding assay (adapted from Pellizzoni et al. 2002) was performed. The region containing the first 370 residues of RBM6, consisting of the N-terminal POZ and decamer repeat domains, was translated in vitro in the presence of [^{35}S] methionine and incubated with purified recombinant His-tagged N-terminal RBM6 conjugated to agarose beads. The fraction of ^{35}S-labelled protein bound by the His-tagged protein was then analysed by SDS-PAGE followed by fluorography. The N-terminal ^{35}S-labelled protein was successfully pulled down by the N-terminal His-tag protein (Fig. 7b). When the His-tag alone or agarose beads alone were used, the N-terminal region of RBM6 was not precipitated. To check if the interaction observed was specific, the ability of the His-tagged N-terminal domain to precipitate the unrelated luciferase protein was tested. This protein was shown not to interact with the N-terminal region of RBM6 (Fig. 7b). Taken together, these results suggest that RBM6 is capable of self-interaction that is mediated by the N-terminal region of the protein containing the POZ and decamer repeat domains.

RBM6 is targeted to nascent transcripts

A second major fraction of RBM6 in cultured cells exhibited a diffuse nucleoplasmic distribution rather than being localized in IGC-associated foci. As a potential splicing factor, this former distribution might reflect a population of endogenous RBM6 that interacts with nascent transcripts. To examine this possibility we first asked whether transcriptional inhibition had any consequences for RBM6 localization since a number of studies have revealed that RNA polymerase II, splicing factors and transcription factors redistribute when the transcriptional activity of the nucleus is altered (Spector et al. 1991; Bregman et al. 1995; Dirks et al. 1997; Zeng et al. 1997). We used two transcriptional inhibitors, actinomycin D (ActD) and 5,6-dichloro-1-β-D-ribofuranosylbenzimidazole (DRB), to examine whether the localization of RBM6 was static or responsive to changes in transcriptional activity in three different cell lines (HeLa, COS-7 and NIH3T3). Localization of endogenous RBM6 was examined in cells that had been incubated in medium containing an inhibitor prior to fixation and then immunostained with either antiserum α83 or α84 against RBM6 (Fig. 8a). After transcription inhibition a dramatic reorganization of RBM6 was observed using both antisera, with some of the protein appearing to accumulate in discrete caps at the nucleolar periphery (Fig. 8a; arrows indicate RBM6 at the nucleolus). In addition to the nucleolar accumulation, a subset of the RBM6 remained either as a diffuse nucleoplasmic component (α83), or in enlarged foci (antiserum 84) as in untreated cells. Redistribution of RBM6 was seen with both DRB and actinomycin D treatments, indicating the effects observed most likely resulted from general inhibition of RNA polymerase II.

To assess whether exogenous RBM6 was also sensitive to changes in pre-mRNA transcription, the effect of transcription inhibitors in HeLa cells transiently expressing RBM6-GFP was examined (Fig. 8b). Treatment with actinomycin D for 3 h prior to fixation caused clear changes in the normal distribution of RBM6-GFP. RBM6-GFP showed a dramatic accumulation at the nucleolar periphery, analogous to the response of the endogenous protein, and it also redistributed to a number of round enlarged nuclear foci. Moreover, the diffuse nucleoplasmic distribution of RBM6-GFP decreased significantly, presumably due to this fraction of RBM6 accumulating in the enlarged nuclear foci or at the nucleolar periphery. Similar changes were observed with DRB inhibition and the redistribution of RBM6

was found to be reversible by washing out this inhibitor (data not shown). However, treatment with the translational inhibitor cycloheximide did not induce changes in RBM6 distribution (Fig. 8b). Overall, since inhibiting transcription will decrease the number of primary transcripts present throughout the nucleoplasm, the reduction of diffuse RBM6 staining observed after inhibition is consistent with the loss of a population of RBM6 that is normally complexed with nascent RNA. More direct evidence for this suggestion was obtained by a second approach in which we examined RBM6 localization in transcriptionally active regions of *Xenopus* GVs.

As mentioned above, full-length RBM6 was targeted to LBCs as well as to IGCs in oocyte nuclei. In particular, RBM6 was targeted to the typical lateral loops that project from the chromosomes and that are the defining characteristics of LBCs (Fig. 5). Each lateral loop normally comprises a highly extended region of chromatin that exhibits high levels of pol II transcription and as a result possesses a dense coating of nascent transcripts visible with the light microscope (Fig. 10c). It is also readily apparent in some loops that the "matrix" of nascent RNP is arranged in a gradient of increasing thickness that reflects the increasing length of the transcripts produced by continued transcription elongation. In well-displayed loops from injected oocytes immunostaining of RBM6-His showed that the extent of fluorescence was proportional to the mass of the RNP matrix, the pattern of localization expected if RBM6 interacts with nascent transcripts (Fig. 9). This was particularly evident after co-staining for RBM6 and for RNA polymerase II (pol II). Antibodies against pol II such as mAb H5 identify the transcriptionally active DNA "axis" of loops and produce a thin and even diffraction-limited line of immunostaining that underlies the RNP matrix (Fig. 9; Gall et al. 1999). In preparations co-stained with antibodies against the His-tag and with mAb H5, RBM6 clearly did not co-localize with the pol II transcription complexes attached to the loop axis but followed the mass of the nascent RNP (Fig. 9, merge). Moreover, immunostaining (Fig. 10b) also revealed that RBM6 was associated with the nascent RNP of most clearly visible loops rather than a small subset of transcription units, as might be predicted for a gene-specific splicing factor.

An unexpected effect of exogenous RBM6 expression was a dramatic change in the morphology of many loops; compared with typical loops from uninjected oocytes (Fig. 10c) loops from RBM6-injected oocytes exhibited a highly contorted, rather coiled appearance by phase contrast microscopy (Fig. 10a). Immunostaining showed that this effect was due to a heavy coating of RBM6, with the coiled appearance apparently resulting from a spirally arranged accretion of RBM6 along transcription units (Fig. 10b and inset). In other cases loops appeared to be fused together and collapsed onto the LBC axis rather than being stiffly extended like the coiled loops. We think this aggregation and the heavy, coiled coating of extended loops may be due to the propensity of exogenous RBM6 targeted to nascent transcripts to self-organize into the large multimers as reflected on IGC surfaces as RBM6 beads.

It has also been well established in studies of LBCs from many species that a small number of loops naturally exhibit complex morphologies due to the accretion of either extremely large amounts of RNP (some of whose components may be produced initially at other locations) and/or the formation of an RNP matrix with a distinctive appearance. These "giant" or "marker" loops were particularly prevalent targets of RBM6 in *Xenopus* LBCs (Fig. 5a). Interestingly, the N-terminal deletion mutants of RBM6 (RBM6-CR-His and RBM6-C-His) remained strongly targeted to marker loops whereas they were virtually undetectable in the RNP matrices of typical loops and did not cause any apparent changes in loop morphology. This suggests that oligomerization of RBM6 via the N-terminal domain is necessary for its targeting to the nascent transcripts accessible on typical loops and that the protein/protein and/or RNA:protein interactions brought about by other RBM6 domains, which suffice for IGC targeting, also result in targeting to the unusual RNP accretions on marker loops.

Discussion

RBM6 as a co-transcriptional splicing factor

Using a variety of approaches and cell types we have found that the RNA-binding protein RBM6 can usually be found in association with splicing speckles/IGCs, a distribution supporting a cellular role as a

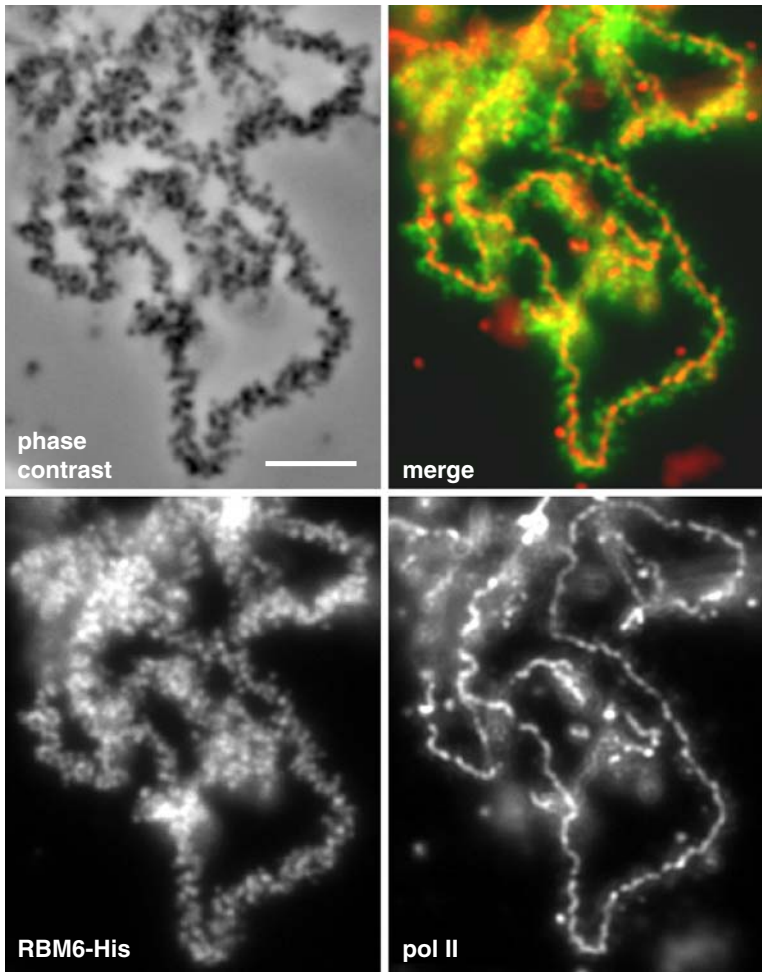

Fig. 9 Association of RBM6 with nascent transcripts in lampbrush chromosome loops. Lampbrush chromosome lateral loops from an oocyte injected 24 h previously with RBM6-His transcripts and co-immunostained with αHis mAb to detect RBM6-His and mAb H5 to detect RNA polymerase II (pol II). In the merged immunostained image pol II in the loop axes is shown in *red* and RBM6-His in the surrounding loop RNP matrix is shown in green. Scale bar, 5 μm

splicing factor that has been inferred in other studies (Bonnal et al. 2008). The co-localization of endogenous RBM6 with IGCs that we observed in mammalian cell lines was also a feature of the targeting of exogenous, N-terminally deleted forms of RBM6 to the IGCs of *Xenopus* oocytes. Interestingly, the site of targeting of full-length RBM6 to IGCs was subtly different in both cell types. In the latter cases RBM6 was associated specifically with the IGC surface, in a manner that, as discussed below, was dependent on its multimerization via a repetitive N-terminal domain. On the other hand, the specificity of localization of all forms of RBM6 to IGCs in general would appear to require specific interactions between one or more IGC components and regions of RBM6 outside the repetitive domain. A second target for RBM6 in oocyte nuclei was the nascent transcripts of active LBCs. However since transcription and nascent transcripts are not found in oocyte IGCs (Gall et al. 1999) it would appear that RBM6 targeting to the IGC surface cannot simply be due to an obligate association with peripherally localized active genes, which are a feature of somatic IGCs. Clearly though, the association of RBM6 with nascent transcripts of LBC transcription units does suggest that RBM6 can have a co-transcriptional mechanism of action, again consistent with a role as a splicing factor. Similarly the related multifunctional RBM protein, RBM4, also appears to act co-transcriptionally in respect to both its roles in splicing and miRNA-related translational repression (Lin and Tarn 2005; Pawlicki and Steitz 2010). Moreover, the targeting of RBM6 to large numbers of LBC loops suggests that the co-transcriptional functions of RBM6 are more widespread than would be anticipated from the limited numbers of genes so far implicated as its

targets. As such this suggests that RBM6 could have a role in the processing or regulation of most transcripts in the manner of a ubiquitously expressed general splicing repressor like hnRNPA1 or PTB (hnRNPI) rather than being a cell-type-restricted activator of alternative splicing of a specific subset of genes. Furthermore RBM6 associated with LBC transcription units along their entire length and did not appear localized to any region within nascent transcripts (as is the case for CELF-1; Morgan 2007). This in turn could suggest that the ability of RBM6 to modulate splicing patterns stems from a general packaging role in nascent pre-mRNA effected along the entire transcript length as found for more widespread hnRNPs such as those mentioned above (Wu et al. 1991).

RBM6 multimerization and the formation of novel nuclear structures

One surprising property of RBM6 was the ability of the exogenous, full-length protein, but not of endogenous or N-terminally deleted RBM6, to form globular structures at the periphery of IGCs in both mammalian cultured cells (RBM6 bodies) and in GVs (RBM6 beads). We found that the apparent exclusion of RBM6 from the IGC interior in these cases was dependent on its N-terminal domain, which drives the self-interaction required for de novo formation of the large RBM6-containing structures. We do not know why endogenous RBM6 does not form such structures but it may be that a higher abundance, or an unregulated or inappropriately modified state allows exogenous full-length RBM6 to multimerize and form large nuclear bodies. It might also be that most endogenousRBM6 is produced from alternatively spliced mRNAs that lack the N-terminal domain. The N-terminal domain is not found in other RBM proteins, but has a conserved organization in RBM6, being composed of about 20 decapeptide repeats in the mouse, human and *Xenopus tropicalis* orthologues. Although the decapeptide repeat sequence is rather different in each species, the repeat consensus sequences all have a central arginine residue. We have found that mouse RBM6 is able to form large nuclear structures in mammalian and amphibian nuclei, so the multimerization function of its N-terminal region is presumably a conserved feature of the repetitive domain.

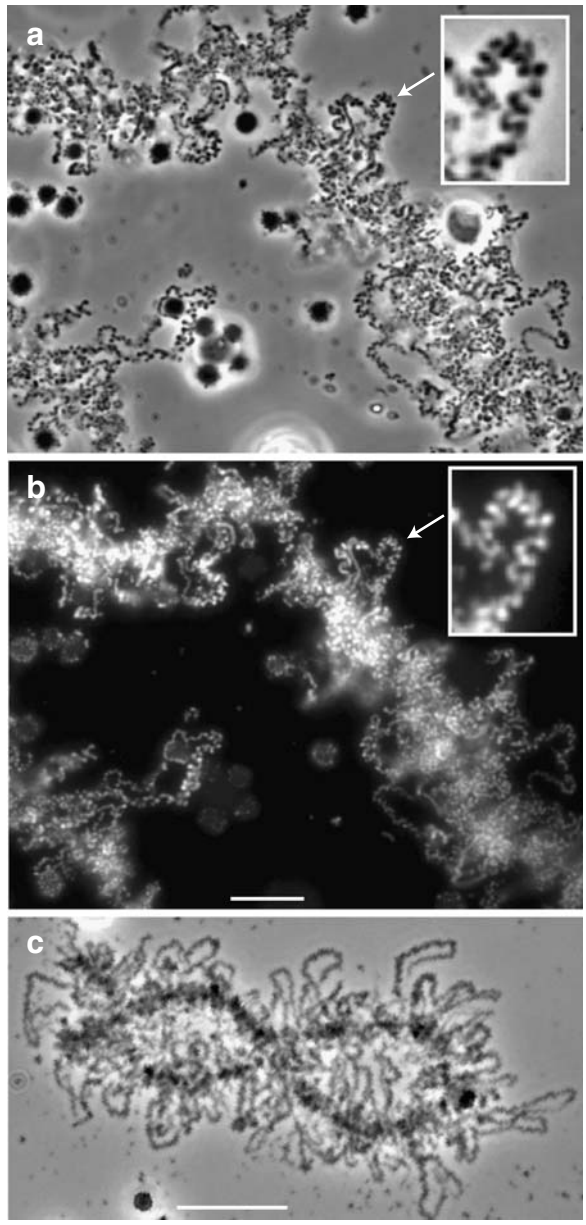

Fig. 10 Altered morphology of active transcription units induced by RBM6. **a**, **b** Phase contrast and fluorescent images, respectively, of a portion of a lampbrush chromosome from an oocyte injected 48 h previously with transcripts encoding RBM6-His.The drastic alteration in loop morphology brought about by RBM6 is apparent by comparison of (**a**) to the phase contrast image of a fixed lampbrush bivalent isolated from an uninjected oocyte (**c**). The inset in (**a**) is an enlargement of a portion of a loop (indicated by the *arrow*) that illustrates the characteristic spiral morphology of RBM6-affected loops. Immunostaining with αHis mAb in (**b**) confirms the accumulation of the protein in spiral loops, and the *inset* contains an enlargement of the same loop inset in (**a**). Scale bars, 10 μm

For several reasons we think the formation of nuclear structures by exogenous RBM6 in vivo may provide some useful analogies for understanding the biogenesis of other nuclear bodies. For instance, as well as their overall morphological resemblance to bona fide nuclear bodies, RBM6 structures specifically associated with IGCs. Such pairwise associations are well known among other types of nuclear body (examples are the association of GEMs with CBs and CBs with nucleoli in somatic cells and CBs with IGCs in GVs). Moreover, comparison of the many RBM6 nuclear bodies formed on the surface of oocyte IGCs and the fewer found at the periphery of mammalian cultured cell IGCs, shows them to be of similar size and morphology. The existence of a self-limited size range among a given type of nuclear body is a good indicator that they form by self-organization (Misteli 2008) and we think that this principle also underlies the de novo formation of RBM6-containing structures. Finally, like RBM6, the diagnostic marker/signature proteins of classic nuclear bodies, such as SMN, PML, Cajal and Sam 68 bodies, have the capacity to self-interact (Hebert and Matera 2000).

Recent findings argue against an obvious model in which self-interacting marker proteins simply provide a pre-existing, dynamic physical scaffold that then sequesters the variety of functional components found in each type of body (Kaiser et al. 2008). This conclusion arises because CB components other than the marker protein, coilin, have also been shown to be capable of nucleating the formation of typical CBs (Tuma and Roth 1999; Kaiser et al. 2008). Nonetheless it has also been found using coilin-null mutants that the absence of coilin leads to the failure of CBs to form in *Drosophila* (Liu et al. 2009) and *Arabidopsis* (Collier et al. 2006) and to the fragmentation of CBs in mouse cells (Tucker et al. 2001). Moreover, removing coilin's N-terminal self-interaction domain prevents its incorporation into pre-existing CBs (Bohmann et al. 1995; Hebert and Matera 2000) in the same way that we have found the absence of the RBM6 multimerization domain prevents formation of both types of RBM6 nuclear bodies. So although coilin is still believed to have a key role in organizing CBs, rather than this being via the provision of a pre-organized scaffold it may instead act to stabilise the transient interactions of other CB components, any of which can themselves nucleate the self-organization of a CB. In the case of the structures that are formed by exogenous RBM6 we do not know if they consist exclusively or predominantly of this protein or contain a range of components. However, the relatively uniform morphology that may be imparted by just this single component raises the possibility that for other types of nuclear body, their signature protein is the key determinant of the characteristic morphological properties (average size, shape and pairing with other nuclear bodies) and biophysical characteristics (viscosity, density, and refractive index) of that body once formed in a given nucleus. In principle this could be tested by determining if a structure with the physical characteristics of, for instance, a normal CB (which would clearly be different for example from those of an RBM6 bead) could be generated in GVs simply by overexpressing coilin in the absence of the other non-structural, functional CB components. Unfortunately, given the large variety and abundance of the latter (especially in GVs) this is not a straightforward experiment.

A second major change in the morphology of nuclear structures that was brought about by multimerized RBM6 was seen among LBC loops. The active transcription units of "normal" loops typically appear to have a linear, extended axis surrounded by a light "feathery" RNP matrix comprising the nascent transcripts; the matrix can sometimes be seen to increase in mass along the loop concomitant with the polarity of transcription and transcript growth. However the targeting of RBM6 to the loop RNP brought about effects that ranged from a general increase in loop mass, through to the accretion of sufficient RBM6 to produce a phase-dense matrix and an apparently distorted loop shape, and ultimately led to loops in which the accumulation of large amounts of RBM6 caused loop aggregation and collapse onto the main body of the chromosome. The intermediate condition described for RBM6-containing matrices proved to be particularly intriguing; often such loops had an overtly spiral or zigzag appearance when viewed either by phase contrast or by immunostaining of the tagged RBM6. To our knowledge the creation of such a distinctive loop morphology by exogenous proteins is a unique feature of RBM6; a large number of transcript-binding components have previously been expressed in oocytes, such as snRNP and hnRNP proteins and including another self-interacting protein, xNF7 (Beenders et al. 2007), but dramatic changes in loop morphology have not been reported. On close examination the spiral loop morphology caused by RBM6 did not appear simply to be due to the loop

itself following a spiral track in space but owed more to the disposition of a heavy loop matrix arranged spirally around the loop. Our inability to detect N-terminally deleted forms of RBM6 in the nascent transcripts of typical loops suggests that the oligomerization that is driven by the N-terminal domain is a key feature in imparting this novel loop morphology. Indeed, in some cases the loop matrix itself clearly appeared to be formed by fusion of granules with similar dimensions to the RBM6 beads observed on the surfaces of the IGCs. The distinctive spiral arrangement of RBM6-containing loop matrix bears a striking resemblance to electron microscopic observations of normal loop matrices. The basic structural units of nascent transcripts observed by e.m. are small particles 20–30 nm in diameter. These particles can aggregate to a greater or lesser extent such that in some loops they form higher order particles or globules large enough to be resolved by the light microscope and imparting a characteristic morphology to the matrices of those loops (reviewed in Callan 1986). Moreover, in the scanning electron microscope studies of Angelier et al. 1984 it is clear that the RNP particles or "bodies" of various dimensions are arranged helically around loop axes and that in cases where larger bodies form by aggregation their close packing causes the formation of a "continuous spiral sleeve encircling the loop axis". The latter description also accurately portrays the effect of RBM6 on loop morphology that we observed with the light microscope and we conclude that this unique morphological effect ultimately reflects the spiral arrangement of nascent RNP around highly active transcription units that is not normally apparent. It appears then that the targeting of large RBM6 multimers to nascent transcripts can reveal an aspect of the topological organization of transcripts in active transcription units at the light microscope level.

Acknowledgements We are grateful to Rivka Dikstein for RBM6 antibodies and to Archa Fox and Angus Lamond for help with the analysis of paraspeckles. We also thank Tim Self for assistance with confocal microscopy and the MRC for a studentship to support EH.

References

Andrade LE, Chan EK, Raska I, Peebles CL, Roos G, Tan EM (1991) Human autoantibody to a novel protein of the nuclear coiled body: immunological characterization and cDNA cloning of p80-coilin. J Exp Med 173:1407–1419

Angelier N, Paintraud M, Lavaud A, Lechaire JP (1984) Scanning electron microscopy of amphibian lampbrush chromosomes. Chromosoma 89:243–253

Beenders B, Jones PL, Bellini M (2007) The tripartite motif of nuclear factor 7 is required for its association with transcriptional units. Mol Cell Biol 27:2615–2624

Black DL (2003) Mechanisms of alternative pre-messenger RNA splicing. Annu Rev Biochem 72:291–336

Bohmann K, Ferreira JA, Lamond AI (1995) Mutational analysis of p80 coilin indicates a functional interaction between coiled bodies and the nucleolus. J Cell Biol 131:817–831

Bonnal S, Martinez C, Forch P, Bachi A, Wilm M, Valcarcel J (2008) RBM5/Luca-15/H37 regulates Fas alternative splice site pairing after exon definition. Mol Cell 32:81–95

Bregman DB, Du L, van der Zee S, Warren SL (1995) Transcription-dependent redistribution of the large subunit of RNA polymerase II to discrete nuclear domains. J Cell Biol 129:287–298

Caceres JF, Misteli T, Screaton GR, Spector DL, Krainer AR (1997) Role of the modular domains of SR proteins in subnuclear localization and alternative splicing specificity. J Cell Biol 138:225–238

Callan HG (1986) Lampbrush chromosomes. Springer, Berlin

Chan EK, Takano S, Andrade LE, Hamel JC, Matera AG (1994) Structure, expression and chromosomal localization of human p80-coilin gene. Nucleic Acids Res 22:4462–4469

Collier S, Pendle A, Boudonck K, van Rij T, Dolan L, Shaw P (2006) A distant coilin homologue is required for the formation of Cajal bodies in Arabidopsis. Mol Biol Cell 17:2942–2951

Cook PR (1999) The organization of replication and transcription. Science 284:1790–1795

Daneholt B (2001) Assembly and transport of a premessenger RNP particle. Proc Natl Acad Sci USA 98:7012–7017

Dirks RW, de Pauw ES, Raap AK (1997) Splicing factors associate with nuclear HCMV-IE transcripts after transcriptional activation of the gene, but dissociate upon transcription inhibition: evidence for a dynamic organization of splicing factors. J Cell Sci 110:515–522

Doyle O, Corden JL, Murphy C, Gall JG (2002) The distribution of RNA polymerase II largest subunit (RPB1) in the *Xenopus* germinal vesicle. J Struct Biol 140:154–166

Drabkin H, West J, Hotfilder M et al (1999) DEF-3(g16/NY-LU-12), an RNA binding protein from the 3p21.3 homozygous deletion region in SCLC. Oncogene 18:2589–2597

Fox AH, Lam YW, Leung AK et al (2002) Paraspeckles: a novel nuclear domain. Curr Biol 12:13–25

Fu XD, Maniatis T (1992) Isolation of a complementary DNA that encodes the mammalian splicing factor SC35. Science 256:535–538

Fu XD, Mayeda A, Maniatis T, Krainer AR (1992) General splicing factors SF2 and SC35 have equivalent activities in vitro, and both affect alternative 5′ and 3′ splice site selection. Proc Natl Acad Sci USA 89:11224–11228

Fushimi K, Ray P, Kar A, Wang L, Sutherland LC, Wu JY (2008) Up-regulation of the proapoptotic caspase 2 splicing isoform by a candidate tumor suppressor, RBM5. Proc Natl Acad Sci USA 105:15708–15713

Gall JG (1991) Spliceosomes and snurposomes. Science 252:1499–1500

Gall J (1998) Spread preparation of *Xenopus* germinal vesicle contents. In: Spector D, Goldman R, Leinwand L (eds) Cells: a laboratory manual, vol 1. Cold Spring Harbor Laboratory Press, Cold Spring Harbor, pp 52.51–52.54

Gall JG (2003) The centennial of the Cajal body. Nat Rev Mol Cell Biol 4:975–980

Gall JG, Bellini M, Wu Z, Murphy C (1999) Assembly of the nuclear transcription and processing machinery: Cajal bodies (coiled bodies) and transcriptosomes. Mol Biol Cell 10:4385–4402

Gall JG, Wu Z, Murphy C, Gao H (2004) Structure in the amphibian germinal vesicle. Exp Cell Res 296:28–34

Hall LL, Smith KP, Byron M, Lawrence JB (2006) Molecular anatomy of a speckle. Anat Rec A Discov Mol Cell Evol Biol 288:664–675

Handwerger KE, Cordero JA, Gall JG (2005) Cajal bodies, nucleoli, and speckles in the *Xenopus* oocyte nucleus have a low-density, sponge-like structure. Mol Biol Cell 16:202–211

Hebert MD, Matera AG (2000) Self-association of coilin reveals a common theme in nuclear body localization. Mol Biol Cell 11:4159–4171

Hock J, Weinmann L, Ender C et al (2007) Proteomic and functional analysis of Argonaute-containing mRNA-protein complexes in human cells. EMBO Rep 8:1052–1060

Hotfilder M, Baxendale S, Cross M, Sablitzky F (1999) Def-2, -3, -6 and -8, novel mouse genes differentially expressed in the haemopoietic system. Br J Haematol 106:335–344

Inoue A, Tsugawa K, Tokunaga K et al (2008) S1-1 nuclear domains: characterization and dynamics as a function of transcriptional activity. Biol Cell 100:523–535

Kaiser TE, Intine RV, Dundr M (2008) De novo formation of a subnuclear body. Science 322:1713–1717

Laemmli U (1970) Cleavage of structural proteins during the assembly of the head of bacteriophage T4. Nature 227:680–685

Lai MC, Kuo HW, Chang WC, Tarn WY (2003) A novel splicing regulator shares a nuclear import pathway with SR proteins. EMBO J 22:1359–1369

Lerner EA, Lerner MR, Janeway CA Jr, Steitz JA (1981) Monoclonal antibodies to nucleic acid-containing cellular constituents: probes for molecular biology and autoimmune disease. Proc Natl Acad Sci USA 78:2737–2741

Lin JC, Tarn WY (2005) Exon selection in alpha-tropomyosin mRNA is regulated by the antagonistic action of RBM4 and PTB. Mol Cell Biol 25:10111–10121

Lin JC, Tarn WY (2009) RNA-binding motif protein 4 translocates to cytoplasmic granules and suppresses translation via argonaute2 during muscle cell differentiation. J Biol Chem 284:34658–34665

Liu JL, Wu Z, Nizami Z et al (2009) Coilin is essential for Cajal body organization in *Drosophila melanogaster*. Mol Biol Cell 20:1661–1670

Matera AG, Shpargel KB (2006) Pumping RNA: nuclear bodybuilding along the RNP pipeline. Curr Opin Cell Biol 18:317–324

Matera AG, Izaguire-Sierra M, Praveen K, Rajendra TK (2009) Nuclear bodies: random aggregates of sticky proteins or crucibles of macromolecular assembly? Dev Cell 17:639–647

Misteli T (2007) Beyond the sequence: cellular organization of genome function. Cell 128:787–800

Misteli T (2008) Cell biology: nuclear order out of chaos. Nature 456:333–334

Morgan GT (2002) Lampbrush chromosomes and associated bodies: new insights into principles of nuclear structure and function. Chromosome Res 10:177–200

Morgan GT (2007) Localized co-transcriptional recruitment of the multifunctional RNA-binding protein CELF1 by lampbrush chromosome transcription units. Chromosome Res 15:985–1000

Pawlicki JM, Steitz JA (2010) Nuclear networking fashions pre-messenger RNA and primary microRNA transcripts for function. Trends Cell Biol 20:52–61

Pellizzoni L, Baccon J, Rappsilber J, Mann M, Dreyfuss G (2002) Purification of native survival of motor neurons complexes and identification of Gemin6 as a novel component. J Biol Chem 277:7540–7545

Prasher DC, Eckenrode VK, Ward WW, Prendergast FG, Cormier MJ (1992) Primary structure of the *Aequorea victoria* green-fluorescent protein. Gene 111:229–233

Pyne CK, Simon F, Loones MT, Geraud G, Bachmann M, Lacroix JC (1994) Localization of antigens PwA33 and La on lampbrush chromosomes and on nucleoplasmic structures in the oocyte of the urodele *Pleurodeles waltl*: light and electron microscopic immunocytochemical studies. Chromosoma 103:475–485

Roth MB, Murphy C, Gall JG (1990) A monoclonal antibody that recognizes a phosphorylated epitope stains lampbrush chromosome loops and small granules in the amphibian germinal vesicle. J Cell Biol 111:2217–2223

Schultz J, Milpetz F, Bork P, Ponting CP (1998) SMART, a simple modular architecture research tool: identification of signaling domains. Proc Natl Acad Sci USA 95:5857–5864

Singh OP, Visa N, Wieslander L, Daneholt B (2006) A specific SR protein binds preferentially to the secretory protein gene transcripts in salivary glands of *Chironomus tentans*. Chromosoma 115:449–458

Smith AJ, Ling Y, Morgan GT (2003) Subnuclear localization and Cajal body targeting of transcription elongation factor TFIIS in amphibian oocytes. Mol Biol Cell 14:1255–1267

Spector DL (1993) Nuclear organization of pre-mRNA processing. Curr Opin Cell Biol 5:442–447

Spector DL, Fu XD, Maniatis T (1991) Associations between distinct pre-mRNA splicing components and the cell nucleus. EMBO J 10:3467–3481

Sutherland H, Bickmore WA (2009) Transcription factories: gene expression in unions? Nat Rev Genet 10:457–466

Sutherland LC, Rintala-Maki ND, White RD, Morin CD (2005) RNA binding motif (RBM) proteins: a novel family of apoptosis modulators? J Cell Biochem 94:5–24

Tucker KE, Berciano MT, Jacobs EY et al (2001) Residual Cajal bodies in coilin knockout mice fail to recruit Sm snRNPs and SMN, the spinal muscular atrophy gene product. J Cell Biol 154:293–307

Tuma RS, Roth MB (1999) Induction of coiled body-like structures in *Xenopus oocytes* by U7 snRNA. Chromosoma 108:337–344

Warren SL, Landolfi AS, Curtis C, Morrow JSW (1992) Cytostellin: a novel, highly conserved protein that undergoes continuous redistribution during the cell cycle. J Cell Sci 103:381–388

Wu ZA, Murphy C, Callan HG, Gall JG (1991) Small nuclear ribonucleoproteins and heterogeneous nuclear ribonucleoproteins in the amphibian germinal vesicle: loops, spheres, and snurposomes. J Cell Biol 113:465–483

Zeng C, Kim E, Warren SL, Berget SM (1997) Dynamic relocation of transcription and splicing factors dependent upon transcriptional activity. EMBO J 16:1401–1412